Linear stability analysis of Poiseuille-Rayleigh-Bénard flows in binary fluids with Soret effect

J. Hu, H. Ben Hadid, and D. Henry[a)]
Laboratoire de Mécanique des Fluides et d'Acoustique, UMR CNRS 5509, Ecole Centrale de Lyon/ Université Claude Bernard Lyon 1/INSA de Lyon, ECL, 36 Avenue Guy de Collongue, 69134 Ecully Cedex, France

(Received 5 May 2006; accepted 18 January 2007; published online 9 March 2007)

Temporal and spatiotemporal instabilities of Poiseuille-Rayleigh-Bénard flows in binary fluids with Soret effect have been investigated by a Chebyshev collocation method. Both situations corresponding to the fluid layer heated from below or from above have been studied. When heating is from below and for positive separation factors, the critical thresholds strongly increase when the throughflow is applied, and the boundary curves between absolute and convective instabilities (AI/CI) increase as well, but more steeply. For large enough positive separation factors, there exist three local minima in the neutral curves Ra(k) (Rayleigh number against wavenumber) for moderate Reynolds numbers (Re), which results in the discontinuity of the critical wavenumber curve and the nonsmoothness of the critical Rayleigh number curve when the Reynolds number is varied. For negative separation factors, there exists a contact point between the critical Rayleigh number curve and the AI/CI boundary curve at which the fluid system is directly changed from stable to absolutely unstable without crossing the convectively unstable region. This contact point has been characterized and localized for different negative separation factors. When heating is from above, the main observation is that the stationary curve obtained at Re=0 is replaced by two critical curves, one stationary and the other oscillatory, when a throughflow is applied. An energy budget analysis for the binary fluid system is also performed. A better insight into the role played by the solutal buoyancy contribution in the different situations is thus obtained. © *2007 American Institute of Physics*. [DOI: 10.1063/1.2709931]

I. INTRODUCTION

Mixed convection in binary mixtures with Soret effect has many practical applications, such as chemical vapor deposition (CVD) in the electronic industry. It also leads to rich and complex spatiotemporal pattern formations, which have a great theoretical interest. In fact, the already rich spatiotemporal behavior of the dissipative structures occurring in binary mixture convection[1] is influenced by the externally imposed throughflow. It is why the Poiseuille-Rayleigh-Bénard flows have been intensively studied for small Reynolds numbers[2–5] by linear, nonlinear, and transient behavior studies dealing with either temporal or spatiotemporal instabilities.

How a horizontal plane Poiseuille shear flow changes linear convection properties in heated binary fluid layers was first investigated by Jung *et al.*[2] They solved the full linear stability equations by a shooting method for realistic top and bottom boundary conditions. From their stability analysis, it is found that the throughflow lifts the Hopf symmetry degeneracy of left and right traveling waves (TW), and the frequencies, bifurcation thresholds, and structural properties of the two TW solution branches—as well as the stationary overturning convection (SOC)—are changed dramatically. Later Büchel and Lücke[3] further studied the effect of a horizontal throughflow with small Reynolds numbers on stationary and traveling wave convective patterns with a Galerkin expansion and a finite-difference numerical method. Bifurcation diagrams of various quantities such as Nusselt number, frequency, and mixing behavior are determined as functions of heating rate and wavenumber for several throughflow rates and Soret coupling strengths for ethanol-water parameters. They also studied the growth dynamics of small convective perturbations into different, strongly nonlinear convective states and the transition between them.

Concerning the study of the absolute and convective instability, the boundary curves separating these two types of instabilities for both negative separation factors (corresponding to the two TW solutions) and positive separation factors (corresponding to the SOC solution) are first plotted as a function of the throughflow rate in the paper of Jung *et al.*[2] Later, Büchel and Lücke[4] studied the spatiotemporal properties of the spatially localized convective perturbations in detail for heated binary fluid layers, with or without throughflow. Fronts and pulse-like wave packets formed out of the three relevant perturbations (two oscillatory ones and a stationary one) are analyzed after evaluating the appropriate saddle points of the three respective dispersion relations of the linear stability equations over the complex wavenumber plane. Recently, Jung and Lücke[5] further compared the spatiotemporal properties of fronts that were obtained from the saddle point analysis of the dispersion relation of the linear

[a)]Author to whom correspondence should be addressed. Electronic mail: daniel.henry@ec-lyon.fr

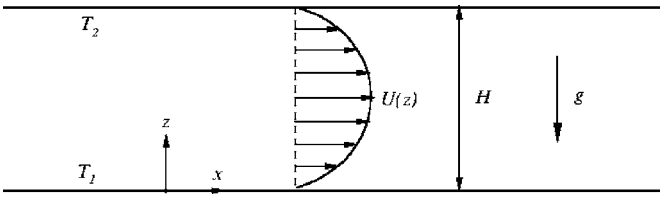

FIG. 1. Schematic representation of the Poiseuille-Rayleigh-Bénard model.

field equations with numerical solutions of the full nonlinear hydrodynamical equations.

In this paper, the linear stability analysis of Poiseuille-Rayleigh-Bénard flows for binary fluids with Soret effect is revisited for a much larger Reynolds number range by a pseudospectral collocation method. The case where the fluid layer is heated from above (a situation which can be unstable for negative separation factors) is also considered. Successively, three different approaches have been used: a temporal stability analysis, a kinetic-energy budget analysis, and a spatiotemporal analysis. In Sec. II, the formulation of the problem is given. In Sec. III, the results of the temporal stability study are first presented for both positive and negative separation factors ψ in the classical situation where the fluid layer is heated from below. Specific behaviors as a jump in wavenumber have been found, and the variation of the thresholds at large Re is better characterized. In the situation where heating is from above, two critical curves, one stationary and the other oscillatory, have been found when a throughflow is applied. Section IV contains the kinetic-energy budget results, which show the evolution of the solutal buoyancy contribution as Re is increased, and indicate the zones where this contribution is effective. The last section gives the boundary curves between absolute and convective instabilities for each of the situations studied. Precisions are given on the point in the parameter space where there is a direct transition from the stable region to the absolutely unstable region.

II. FORMULATION

We consider a nonreactive binary fluid mixture contained in an infinite horizontal channel of height H (Fig. 1). The binary mixture is heated from below or from above: the horizontal boundaries are isothermal and held at different temperatures, T_2 at the top wall ($z=H$) and $T_1 \neq T_2$ at the bottom wall ($z=0$). A throughflow in the x direction is also driven by imposing a constant pressure gradient along the channel. The resulting global flow is usually called the Poiseuille-Rayleigh-Bénard flow.

Due to the influence of the gravitational effect, the binary mixture may become unstable when vertical temperature and concentration gradients exist. To take this into account, the Boussinesq approximation is applied such that density variations are restricted to the buoyancy term and are expressed as a linear law,

$$\rho = \rho_0[1 - \beta_T(T - T_0) - \beta_C(C - C_0)], \tag{1}$$

where β_T and β_C are the thermal and solutal expansion coefficients, and ρ_0, T_0, and C_0 are reference values for density, temperature, and concentration, respectively, which are taken as mean values.

The Soret effect, which arises as the contribution of the temperature gradient to the mass flux, is considered here; whereas the Dufour effect, which arises as the contribution of the concentration gradient to the heat flux, is neglected. The mass flux J_C and the heat flux J_T are then

$$J_C = -\rho_0 D_C \nabla C - \rho_0 D_S \nabla T, \tag{2a}$$

$$J_T = -D_T \nabla T, \tag{2b}$$

where D_C, D_S, and D_T are the solutal diffusion coefficient, Soret diffusion coefficient, and thermal conductivity, respectively. The conductive steady state will then correspond to linear variations along z for both the temperature and concentration, leading to a concentration difference $\Delta C = C_1 - C_2$ (induced by the applied temperature difference $\Delta T = T_1 - T_2$) equal to $-D_S \Delta T / D_C$.

The flow in this system is modeled by the Navier-Stokes equations coupled to an energy equation and a concentration equation. In these equations, length, velocity, time, and pressure are scaled by H, κ/H, H^2/κ, and $\rho_0 \kappa^2/H^2$, respectively (κ is the thermal diffusivity). The dimensionless temperature θ and concentration c are defined as $(T-T_0)/\Delta T$ and $(C-C_0)/\Delta C$. Thus the dimensionless governing equations of the two-dimensional (2D) Poiseuille-Rayleigh-Bénard flow are

$$\nabla \cdot \mathbf{v} = 0, \tag{3a}$$

$$\frac{1}{\mathrm{Pr}}\left(\frac{\partial \mathbf{v}}{\partial t} + \mathbf{v} \cdot \nabla \mathbf{v}\right) = -\frac{1}{\mathrm{Pr}} \nabla p + \nabla^2 \mathbf{v} + \mathrm{Ra}(\theta + \psi c)\mathbf{e}_z, \tag{3b}$$

$$\frac{\partial \theta}{\partial t} + \mathbf{v} \cdot \nabla \theta = \nabla^2 \theta, \tag{3c}$$

$$\frac{\partial c}{\partial t} + \mathbf{v} \cdot \nabla c = \mathrm{Le}(\nabla^2 c - \nabla^2 \theta), \tag{3d}$$

where $\mathbf{v} = (u, w)$ is the two-dimensional dimensionless velocity vector, $\mathbf{e}_z$ is the unit vector in the vertical direction, and the operators are represented as $\nabla = (\partial_x, \partial_z)$ and $\nabla^2 = \partial_x^2 + \partial_z^2$. The dimensionless parameters appearing in the governing system (3) are the Prandtl number, $\mathrm{Pr} = \nu/\kappa$, the Rayleigh number, $\mathrm{Ra} = \beta_T g H^3 \Delta T / \kappa \nu$, the separation factor, $\psi = -\beta_C D_S / \beta_T D_C$, and the Lewis number, $\mathrm{Le} = D_c/\kappa$. Here, ν is the kinematic viscosity. The corresponding boundary conditions are

$$\text{no-slip conditions:} \quad u = w = 0, \quad \text{at } z = 0, 1, \tag{4a}$$

$$\text{thermal conditions:} \quad \theta = 0.5, \quad \text{at } z = 0, \tag{4b}$$

$$\theta = -0.5, \quad \text{at } z = 1, \tag{4c}$$

$$\text{mass impermeability:} \quad \partial_z \eta = 0, \quad \text{at } z = 0, 1, \tag{4d}$$

where $\eta = \theta - c$.

The nondimensional basic steady state can easily be obtained and corresponds to a parabolic z profile for the x com-

ponent of the velocity vector (throughflow), to a constant pressure gradient responsible for this throughflow, and to linear conductive z profiles for temperature and concentration,

$$\bar{u}(z) = -6\,\mathrm{Re}\cdot\mathrm{Pr}(z^2 - z), \tag{5a}$$

$$\nabla\bar{p} = -12\,\mathrm{Re}\cdot\mathrm{Pr}^2\mathbf{e}_x, \tag{5b}$$

$$\bar{\theta}(z) = 0.5 - z, \tag{5c}$$

$$\bar{c}(z) = 0.5 - z, \tag{5d}$$

$$\bar{\eta}(z) = 0. \tag{5e}$$

$\mathrm{Re} = U_0 H/\nu$ is the Reynolds number and U_0 is the dimensional mean velocity obtained by integration over the channel width.

The disturbed two-dimensional Poiseuille-Rayleigh-Bénard flow with Soret effect can be decomposed as $u = \bar{u} + u'$, $w = w'$, $p = \bar{p} + p'$, $\theta = \bar{\theta} + \theta'$, $c = \bar{c} + c'$, and $\eta = \bar{\eta} + \eta'$, and the perturbation quantities can further be expanded as normal modes,

$$(u', w', p', \theta', c', \eta') = [\hat{u}(z), \hat{w}(z), \hat{p}(z), \hat{\theta}(z), \hat{c}(z), \hat{\eta}(z)]e^{i(kx-\omega t)}, \tag{6}$$

where k is a wavenumber and ω a complex pulsation. Substituting them in the governing system (3), we obtain the linear stability equations expressed in primitive variables,

$$ik\hat{u} + D\hat{w} = 0, \tag{7a}$$

$$-i\omega\hat{u} + ik\bar{u}\hat{u} + D\bar{u}\hat{w} = -ik\hat{p} + \mathrm{Pr}(D^2 - k^2)\hat{u}, \tag{7b}$$

$$-i\omega\hat{w} + ik\bar{u}\hat{w} = -D\hat{p} + \mathrm{Pr}(D^2 - k^2)\hat{w} + \mathrm{Pr}\cdot\mathrm{Ra}(\hat{\theta} + \psi\hat{c}), \tag{7c}$$

$$-i\omega\hat{\theta} + ik\bar{u}\hat{\theta} - \hat{w} = (D^2 - k^2)\hat{\theta}, \tag{7d}$$

$$-i\omega\hat{c} + ik\bar{u}\hat{c} - \hat{w} = \mathrm{Le}(D^2 - k^2)(\hat{c} - \hat{\theta}), \tag{7e}$$

where $D = d/dz$. After eliminating $\hat{u}$, $\hat{p}$, and $\hat{c}$ in (7), the linear stability equations which then only depend on the three normal modes ($\hat{w}$, $\hat{\theta}$, and $\hat{\eta}$) are reduced to

$$\mathrm{Pr}\cdot L^2(\hat{w}) + i\omega L(\hat{w}) - ik[\bar{u}L(\hat{w}) - D^2\bar{u}\hat{w}] - \mathrm{Pr}\cdot\mathrm{Ra}\cdot k^2[(1+\psi)\hat{\theta} - \psi\hat{\eta}] = 0, \tag{8a}$$

$$L(\hat{\theta}) - i(\bar{u}k - \omega)\hat{\theta} + \hat{w} = 0, \tag{8b}$$

$$\mathrm{Le}\cdot L(\hat{\eta}) - i(\bar{u}k - \omega)(\hat{\eta} - \hat{\theta}) - \hat{w} = 0, \tag{8c}$$

where $L = D^2 - k^2$. The corresponding linear boundary conditions are

$$\hat{w} = D\hat{w} = 0, \quad \hat{\theta} = 0, \quad D\hat{\eta} = 0 \quad \text{at } z = 0, 1. \tag{9}$$

The linear stability equations (8) are ordinary differential equations in terms of $\hat{w}$, $\hat{\theta}$, and $\hat{\eta}$ and can be regarded as a two-point boundary value problem. If there exists a nontrivial solution for the equations, a corresponding dispersion relation

$$\mathrm{D}(k, \omega; \mathrm{Ra}, \mathrm{Re}, \psi, \mathrm{Pr}, \mathrm{Le}) = 0$$

should be satisfied, and we need to solve an eigenvalue problem. Because it is impossible to find the explicit analytical dispersion relation if there is no further simplification, the dispersion relation has to be obtained numerically. A shooting method has been adopted for this problem in the paper of Jung *et al.*[2] In this paper, the pseudospectral Chebyshev method (Canuto *et al.*[6]) is used to discretize the eigenvalue problem and the QZ algorithm to solve the resulting general eigenvalue problem. From the spectra obtained, we will compute thresholds $\mathrm{Ra}_0(k, \mathrm{Re}, \psi, \mathrm{Pr}, \mathrm{Le})$ (values of Ra for which an eigenvalue has a real part equal to zero whereas all the other eigenvalues have negative real parts) depending on k (here considered as real), but also critical Rayleigh numbers Ra_c by minimization along k [$|\mathrm{Ra}_c| = \inf_{k\in\mathcal{R}}|\mathrm{Ra}_0|(k, \mathrm{Re}, \psi, \mathrm{Pr}, \mathrm{Le})$]. Note that when two eigenmodes are close to critical in a domain of parameters, we will often define a critical Rayleigh number for each of these modes, but it is clear that the true critical Rayleigh number will be given by the minimum of these values.

In the above formulation, we have chosen perturbations with wavenumbers k in the x direction, i.e., two-dimensional perturbations. Let us justify this choice. For the Poiseuille-Rayleigh-Bénard flows in binary fluids, the Squire theorem, which states that two-dimensional disturbances are more dangerous than three-dimensional (3D) ones, is not valid. Nevertheless, as already mentioned by Jung *et al.*,[2] the three-dimensional perturbation problem only depends on $k_x^2 + k_y^2$ and k_x Re, so that the Squire transformation, corresponding to the relations $k^2 = k_x^2 + k_y^2$ and $k\,\mathrm{Re} = k_x\mathrm{Re}_{3\mathrm{D}}$, can be used to make a clear connection between the 3D instability (for arbitrary orientations of the wave vector determining arbitrary values of k_x and k_y) and the 2D instability (transverse waves corresponding to a wave vector k along x). Here, Re is the Reynolds number corresponding to the 2D instabilities considered in the paper, and $\mathrm{Re}_{3\mathrm{D}}$ is the Reynolds number associated with 3D instabilities. This allows to only consider perturbations with wave vectors in the x direction without loss of information. Moreover, some important properties of the 3D instability can be easily derived from the 2D instability analysis for transverse waves, as we will see later. Note first that the throughflow has no influence on the thresholds of the longitudinal instabilities, as, from the second relation, for any value of $\mathrm{Re}_{3\mathrm{D}}$ characterizing the throughflow, the evolution of the longitudinal instability ($k = k_y$, $k_x = 0$) remains similar to what is obtained without throughflow at $\mathrm{Re} = 0$.

III. TEMPORAL INSTABILITY

In the Poiseuille-Rayleigh-Bénard flow with Soret effect, the temporal modes of instability have specific properties: for each real wavenumber k_r, when a complex $\omega = \omega_r + i\omega_i$ is the eigenvalue of the linear stability equations (8), for a Reynolds number Re, then the complex $-\omega^* = -\omega_r + i\omega_i$ is the corresponding eigenvalue for the Reynolds number $-\mathrm{Re}$.

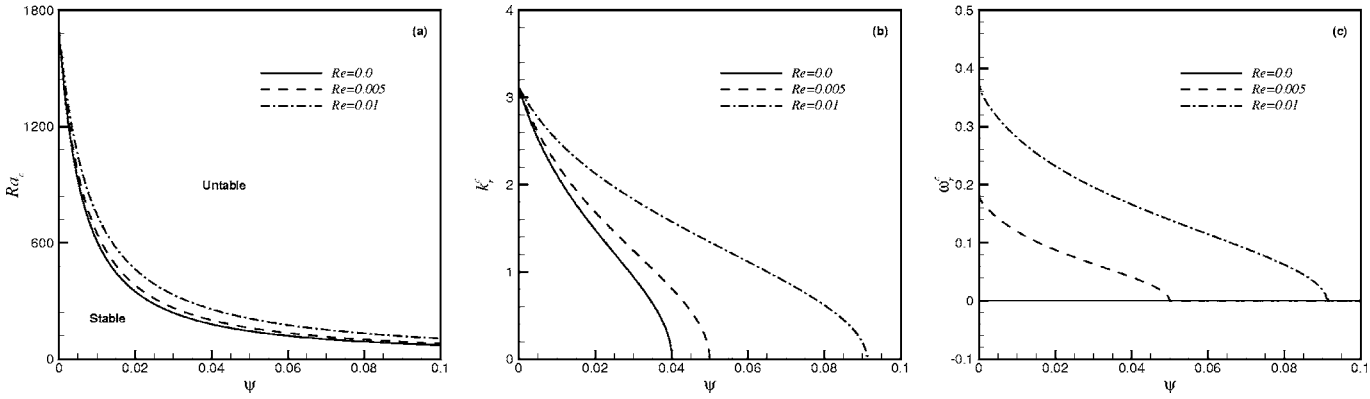

FIG. 2. (a) Critical Rayleigh number Ra_c, (b) real wavenumber k_r^c, and (c) angular frequency ω_r^c as a function of the separation factor ψ for different small Reynolds numbers (Pr=10, Le=0.01).

Here, the asterisk * denotes complex conjugation. This means that without lateral throughflow (Re=0), for the temporal instability, either there exist two modes of unstable waves with equal growth rates but opposite frequencies (oscillatory instability), or there exists only one unstable mode with the zero frequency (stationary instability). For these two types of instability, the relevant critical curves $\mathrm{Ra}_c(\psi)$ have already been exactly plotted by Knobloch and Moore.[7] They solved a complex eight-order polynomial of the underlying eigenvalue problem and identified the existence of a codimension-two bifurcation point at $\psi=\psi_2<0$, which has also been studied in detail with amplitude equations by Cross and Kim[8,9] and Schöpf and Zimmermann.[10,11] In order to validate our results, we have computed the critical curves $\mathrm{Ra}_c(\psi)$ for Re=0 for both Pr=10, Le=0.01 (liquids such as ethanol-water mixture) and Pr=1, Le=0.5 (gases such as ^{3}He-^{4}He mixtures). The results in both cases compare very well with those given in the literature.

In this section, the throughflow is taken into account, but, due to the importance of the Dufour effect[12–14] in binary gas mixtures, only the liquid case at Pr=10 and Le=0.01 is studied in the following sections. For this liquid case, let us recall briefly the main results obtained at Re=0, which are useful for the present study.

For Ra>0 (heating from below) and $\psi<0$, the critical branch corresponds to symmetric left and right traveling waves which induce the onset of oscillatory convection. This Ra_c branch increases slowly with increasing $|\psi|$, and the corresponding critical wavenumber k_r^c increases too, but very slowly, being close to 3.12. At $\psi=\psi^\star$, slightly negative but very close to zero for liquids, there is a transition from TW to a stationary overturning convection. For the onset of this stationary convection (which is well known to be at $\mathrm{Ra}_c=1707.76$ and $k_r^c=3.116$ for $\psi=0$), the critical Rayleigh number and the critical wavenumber change much faster with ψ, decreasing very quickly with increasing ψ, the wavenumber even going to zero at a cutoff separation factor ψ_c [$\psi_c=0.04$ for Pr=10, Le=0.01 (Ref. 7)]. In the region where $k_r^c=0$ ($\psi>\psi_c$), which is known to correspond to a solutal-dominated regime, there is an analytical expression for the critical curve which is $\mathrm{Ra}_c=720\mathrm{Le}/\psi$. Finally, the onset of the stationary convection can also be obtained when heating is from above (Ra<0) and $\psi<0$. In this case, k_r^c is still zero and the thresholds are given by the same analytical expression as in the case $\psi>0$.

A. Ra>0 and $\psi>0$

We first investigate the influence of small Reynolds numbers on the critical Rayleigh number Ra_c, the corresponding real wavenumber k_r^c, and the angular frequency ω_r^c, when heating is from below (Ra>0) and for positive separation factors ($0\leq\psi\leq0.1$) (Fig. 2). It is found that the throughflow induces an increase of the critical Rayleigh number [Fig. 2(a)]. The cutoff separation factor (above which the instability occurs at zero wavenumber) increases quickly with the increase of the Reynolds number [Fig. 2(b)]. With the presence of the throughflow, the otherwise stationary instability becomes oscillatory with a nonzero angular frequency decreasing with the increase of the separation factor [Fig. 2(c)]. Only in the small domain beyond the cutoff separation factor (corresponding to small values of Re and sufficiently large ψ) the instability can still be found as stationary despite the throughflow.

In order to study in detail the influence of much larger inertia effects, we plot the critical curves in Fig. 3 in a larger range of Reynolds number (Re≤5). For small separation factors ($\psi=0.01$ and $\psi=0.05$), the critical Rayleigh number first strongly increases with the increase of the Reynolds number, then evolves more slowly beyond some value of Re [Fig. 3(a)]. For larger separation factors ($\psi=0.1$ and $\psi=0.2$), a change of slope still occurs, but in a discontinuous way. This change of slope also corresponds to local changes for the critical wavenumber [Fig. 3(b)] and for the critical angular frequency [Fig. 3(c)]. Discontinuities in the evolutions are even found for $\psi=0.1$ and 0.2. For $\psi=0.1$, the critical wavenumber first strongly decreases with the increase of Re, then jumps to a larger value of wavenumber close to 3.1. On the contrary, for $\psi=0.2$, the critical wavenumber first strongly increases, before jumping down to a smaller value of wavenumber, but the value reached is still close to 3.1. Similar behaviors are found for the critical angular frequency. The Reynolds number where this change occurs becomes large when the separation factor increases. It then still

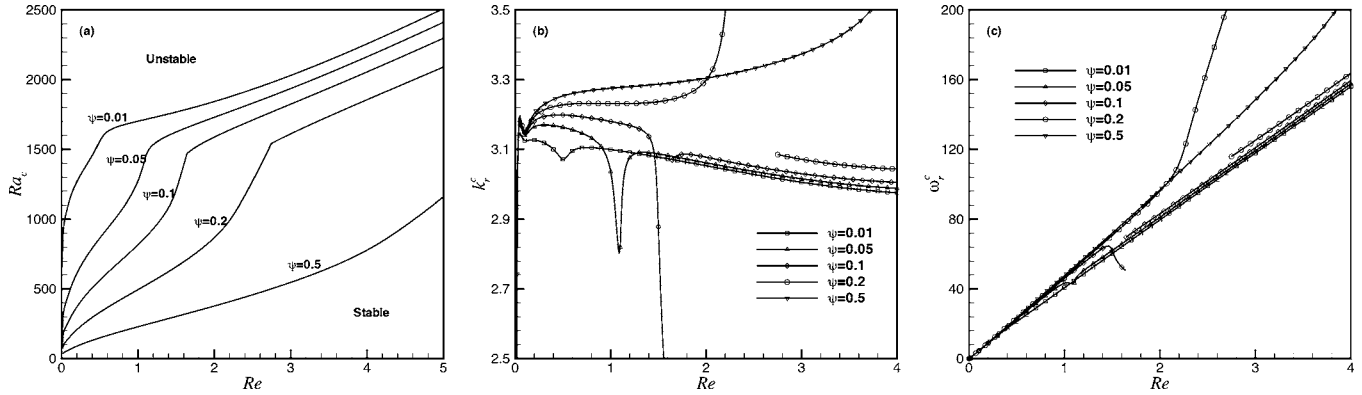

FIG. 3. (a) Critical Rayleigh number Ra_c, (b) real wavenumber k_r^c, and (c) angular frequency ω_r^c as a function of the Reynolds number for different positive values of the separation factor ψ (Pr=10, Le=0.01).

exists for $\psi=0.5$, but cannot be seen in Fig. 3 in the plotted range of Re. Finally, for large enough Reynolds numbers beyond these zones of discontinuities, the critical wavenumber and the critical angular frequency only slightly depend on ψ.

In order to investigate this phenomenon of discontinuity, we plot the neutral curves of the Rayleigh number versus the real wavenumber for increasing Reynolds numbers near the transition in Figs. 4(a) and 5(a) for $\psi=0.1$ and $\psi=0.2$, respectively. For $\psi=0.1$, when Re=1.5 there is only one minimum at $k_r=2.88$, this wavenumber decreasing with the increase of the Reynolds number; when Re=1.54 another local minimum appears at a larger wavenumber $k_r=3.97$; when Re=1.6 a third local minimum occurs at an intermediate wavenumber $k_r=3.02$; then for larger Reynolds numbers there exist three local minima in the neutral curves. Similarly, for $\psi=0.2$, when Re=2.2 there is only one minimum at $k_r=3.49$, this wavenumber increasing with the increase of the Reynolds number; when Re=2.35 two other local minima appear almost simultaneously at two smaller wavenumbers $k_r=2.39$ and $k_r=3.1$. The evolutions with Re of the wavenumbers corresponding to the three local minima are given for both cases in Figs. 4(b) and 5(b). In each case, the global minimum (which gives the critical conditions) corresponds first to the wavenumber branch given as a dotted line, and the transition (indicated by a dashed arrow) occurs towards the middle wavenumber branch with a clear jump in wavenumbers.

We finally give a comment on the three-dimensional instabilities. For the two-dimensional instabilities, the critical Rayleigh number has been found to increase with the increase of the Reynolds number Re. From the Squire transformation, it is clear that for any Reynolds number Re_{3D} associated with a three-dimensional instability, the smallest critical Rayleigh number will be obtained at Re=0, i.e., for $k_x=0$, which means that this minimum critical Rayleigh number will correspond to the longitudinal instability, an instability which is insensitive to the throughflow. The thresh-

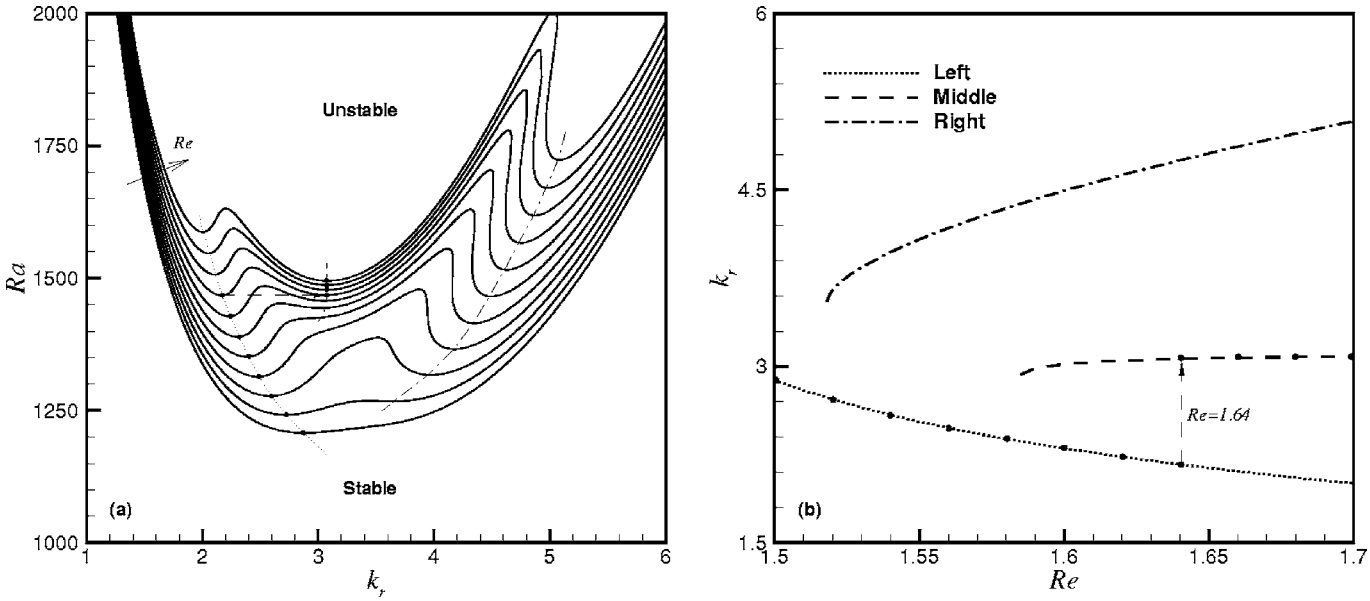

FIG. 4. (a) Neutral curves (Rayleigh number as a function of real wavenumber) for different Reynolds numbers, $\mathrm{Re}=1.5+n\times0.02$ for $n=0$ to 10 (Ra increases with Re as indicated by the arrow) with lines indicating the paths of the local minima. (b) Real wavenumber as a function of the Reynolds number for each local minimum Rayleigh number of the neutral curves (case $\psi=0.1$, Pr=10, Le=0.01). The black dots and dashed arrow indicate the path of the critical values.

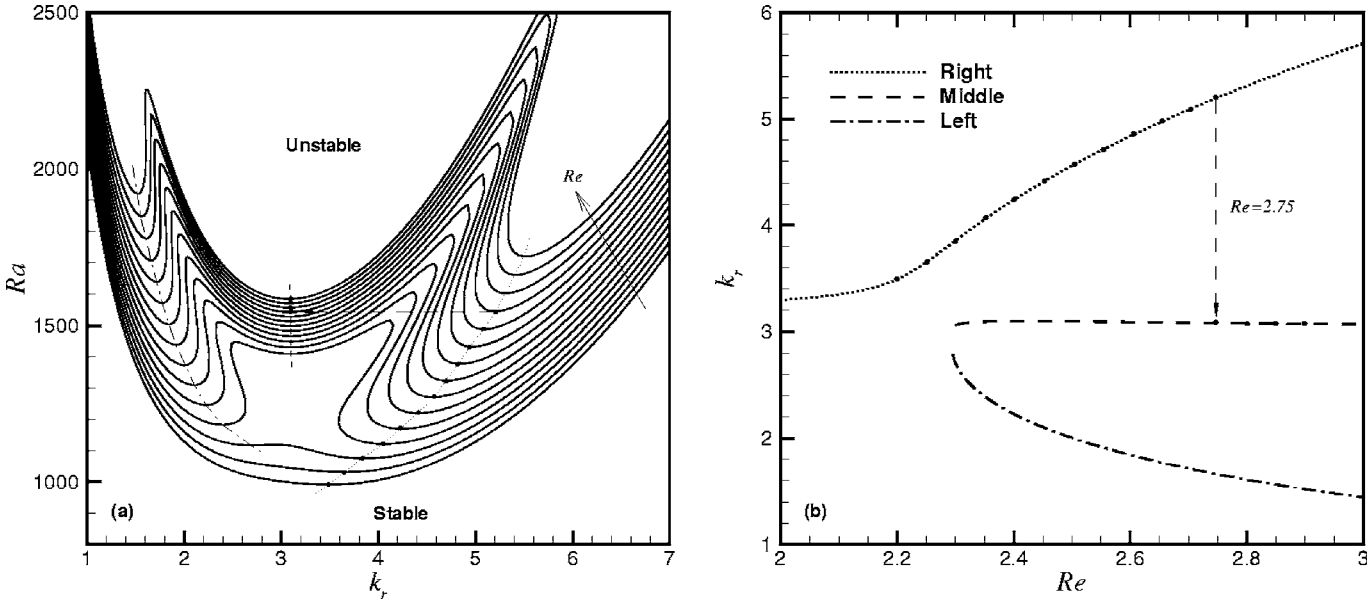

FIG. 5. (a) Neutral curves (Rayleigh number as a function of real wavenumber) for different Reynolds numbers, $\mathrm{Re}=2.2+n\times0.05$ for $n=0$ to 14 (Ra increases with Re as indicated by the arrow) with lines indicating the paths of the local minima. (b) Real wavenumber as a function of the Reynolds number for each local minimum Rayleigh number of the neutral curves (case $\psi=0.2$, $\mathrm{Pr}=10$, $\mathrm{Le}=0.01$). The black dots and dashed arrow indicate the path of the critical values.

olds for oblique waves can also be easily deduced from the two-dimensional thresholds using the Squire transformation.

B. Ra>0 and $\psi<0$

For $\mathrm{Re}=0$, $\mathrm{Ra}>0$, and $\psi<0$, left and right traveling waves have already been identified. They are usually known as upstream ($\omega_r^c<0$) and downstream ($\omega_r^c>0$) modes, respectively. These two unstable waves have the same temporal growth rate and wave speed but opposite traveling directions, i.e., they are symmetrical. They indeed correspond to the same critical Rayleigh number and the same wavenumber. But, when the throughflow is introduced into the binary fluid system, i.e., $\mathrm{Re}\neq0$, the two temporal modes will correspond to two different values of the critical Rayleigh number, and they will evolve differently with Re and determine two distinct branches. The modes on these two branches will be named upstream (downstream) modes with reference to the negative (positive) value of the pulsation ω_r^c characterizing the branch in the limit $\mathrm{Re}\to0$. Let us introduce negative Reynolds numbers in order to define opposite throughflows. It is found that the critical Rayleigh numbers of the downstream and upstream modes change in a continuous way across the zero Reynolds number, and that the corresponding curves are symmetrical one with the other with respect to $\mathrm{Re}=0$ [Fig. 6(a)]. Similar properties are found for the corresponding wavenumbers and pulsations [Figs. 6(b) and 6(c)]. These symmetry properties are due to the following symmetry of the eigenvalue problem: If $(\omega,\bar{u},\hat{u},\hat{w},\hat{p},\hat{\theta},\hat{c})$ is a solution for a given set of values k, Ra, Le, Pr, and ψ, then $(-\omega^*,-\bar{u},-\hat{u}^*,\hat{w}^*,\hat{p}^*,\hat{\theta}^*,\hat{c}^*)$ is also a solution, where * means complex conjugate. The symmetry properties also express the fact that for given ψ and $|\mathrm{Re}|$, the right traveling wave in a flow with $\mathrm{Re}>0$ is completely equivalent to the left traveling wave in a flow with $\mathrm{Re}<0$.

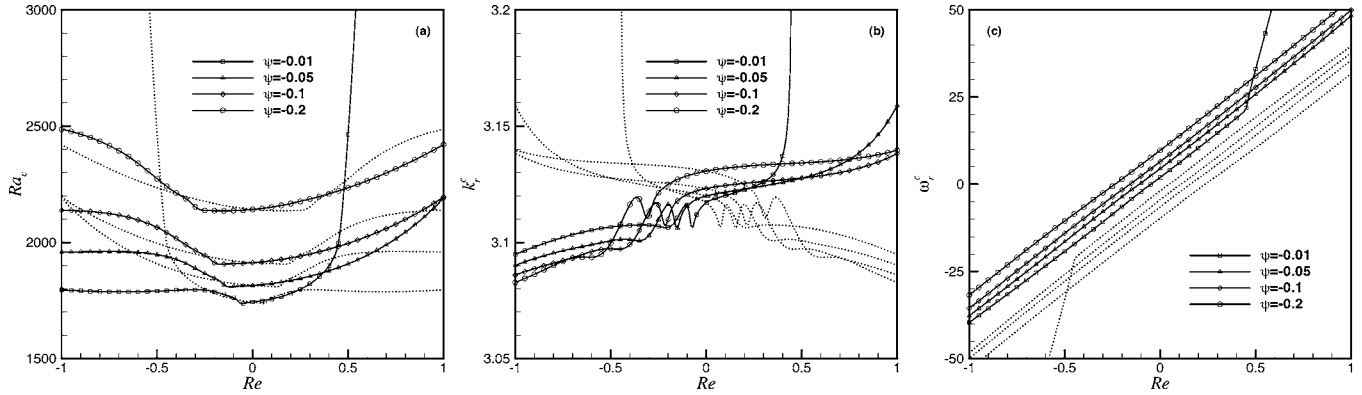

FIG. 6. (a) Critical Rayleigh number Ra_c, (b) real wavenumber k_r^c, and (c) angular frequency ω_r^c as a function of the Reynolds number for different negative values of the separation factor ψ ($\mathrm{Pr}=10$, $\mathrm{Le}=0.01$). The solid lines with symbols correspond to downstream modes and the dotted lines to upstream modes, when Re is positive.

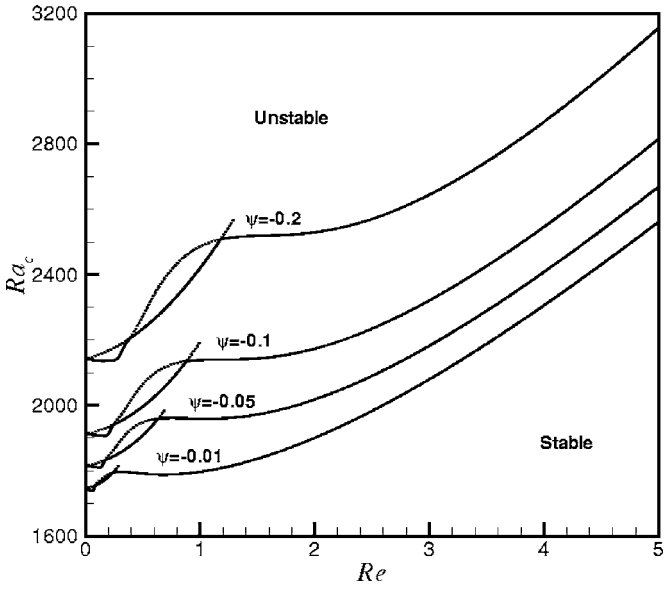

FIG. 7. Critical Rayleigh number curves for both upstream and downstream modes as a function of the Reynolds number for different negative values of the separation factor ψ (Pr=10 and Le=0.01). The critical curves of both modes intersect and the solid line gives the true minimum critical value.

For any value of ψ, as we have two different modes, the true critical Rayleigh number obtained when increasing Re is determined by the smaller of the two thresholds and is shown as a solid line in Fig. 7. From this figure, and as already shown by Jung *et al.*,[2] we see that, when increasing Re from zero, the critical Rayleigh number is first determined by the upstream mode, then the downstream mode becomes the critical mode in an intermediate range of Re; and finally, for larger Re, the upstream mode is again the critical mode. The real critical threshold is found to increase as ψ is decreased, and the Re ranges over which the upstream and downstream modes are first critical increase as well. By observation of Fig. 6(c), we may remark that when Re increases, the pulsation of the upstream mode quickly becomes positive, indicating that the corresponding wave will then travel downstream in the laboratory frame. Concerning the wavenumber [Fig. 6(b)], the wavy variation observed in a small range of Re was already mentioned by Jung *et al.*[2] The evolution of the critical wavenumber and pulsation for larger Re ($1 \leq \mathrm{Re} \leq 5$) is in continuity with what is shown in Figs. 6(b) and 6(c). The wavenumber decreases as Re is increased, but this decrease levels off for Re values around 5, corresponding to values of k_r^c around 2.925. As for the pulsation, it continues to increase almost linearly as Re is increased, reaching for Re=5 values around 190.

From these results, we see that the smallest critical Rayleigh number which is determined by the upstream mode occurs at a small Reynolds number (denoted as Re_m and corresponding to k_m). From the Squire transformation applied at this threshold, it can be written that $k_x\ \mathrm{Re}_{3D}=\mathrm{Re}_m\ k_m$ and $k_x^2+k_y^2=k_m^2$. This shows that for $\mathrm{Re}_{3D}>\mathrm{Re}_m$ the minimum critical Rayleigh number can be obtained by an oblique wave at an angle θ such that $\cos(\theta)=k_x/k_m$ and with $k_x=\mathrm{Re}_m\ k_m/\mathrm{Re}_{3D}$. With the increase of Re_{3D}, the oblique wave angle θ increases then from 0 to $\pi/2$, i.e., the oblique wave evolves from the transverse instability (for $\mathrm{Re}_{3D}=\mathrm{Re}_m$) towards the longitudinal instability (for $\mathrm{Re}_{3D} \gg \mathrm{Re}_m$). But for $\mathrm{Re}_{3D}<\mathrm{Re}_m$, the minimum critical Rayleigh number cannot be reached by any oblique waves, and the critical Rayleigh number in that case will be determined by the pure transverse waves ($k_y=0$, $k_x=k$, $\mathrm{Re}_{3D}=\mathrm{Re}$).

In Ref. 2, the authors pointed out that, for sufficiently large Reynolds numbers, the first bifurcation threshold in binary mixtures asymptotically approaches the critical Rayleigh number $\mathrm{Ra}_c(\mathrm{Re}, \psi=0)$ of a pure fluid with imposed throughflow, for any separation factor ψ, either negative or positive. The critical curves we have obtained for both positive and negative separation factors ψ [Figs. 3(a) and 7], clearly show that this is not the case, as the curves obtained for different values of ψ evolve similarly but do not approach each other when Re becomes large.

C. Ra<0

For negative Rayleigh numbers and negative separation factors, a stationary convection with $k_r^c=0$ was obtained at Re=0. To see the influence of throughflows in this case, we first plot the temporal growth rates and frequencies as functions of the wavenumber for Re=0.04, $\psi=-0.02$, and different negative Rayleigh numbers in Fig. 8. We first see in Fig. 8(a) that the curves giving the temporal growth rates present two maxima which vary as Ra is changed. The maximum in the long wave region determines a critical Rayleigh number (near Ra=3000) which occurs at zero wavenumber with a zero frequency [Fig. 8(b)], whereas the other maximum determines a critical Rayleigh number (near Ra=4000) which occurs at moderate wavenumber (near $k_r=3.6$) with a nonzero frequency. This shows that there exist two critical Rayleigh numbers above which the flow system is linearly unstable: one corresponding to a steady transition similar to that obtained at Re=0, the other corresponding to an oscillatory transition.

In order to investigate the effect of the Reynolds number on the two critical Rayleigh numbers, we plot the critical curves expressed as Ra_c vs ψ for different Reynolds numbers in Figs. 9(a) and 9(b). For Re=0, as already indicated, only a stationary transition is obtained. For $\mathrm{Re} \neq 0$, we see that the two critical curves (stationary and oscillatory) intersect at a negative separation factor. For ψ values smaller than the intersection points, the true critical Rayleigh number is determined by the oscillatory curve whereas for ψ values larger than the intersection points it is determined by the stationary curve. Let us notice that for Re=0.02, the oscillatory curve ends at the point "A." The reason is that the corresponding maximum of the growth rate curve vanishes at that point, and the oscillatory critical Rayleigh number does not then exist further. From the comparison between the results at Re =0.02 and Re=0.04, we see that, when increasing the Reynolds number, both critical curves evolve towards larger $|\mathrm{Ra}_c|$ and $|\psi|$, but the stationary curve evolves more quickly, so that the intersection point occurs at much smaller $|\psi|$. This means that for large enough Reynolds number, the situation heated from above will be difficult to destabilize and the true critical Rayleigh number will correspond to the onset of an

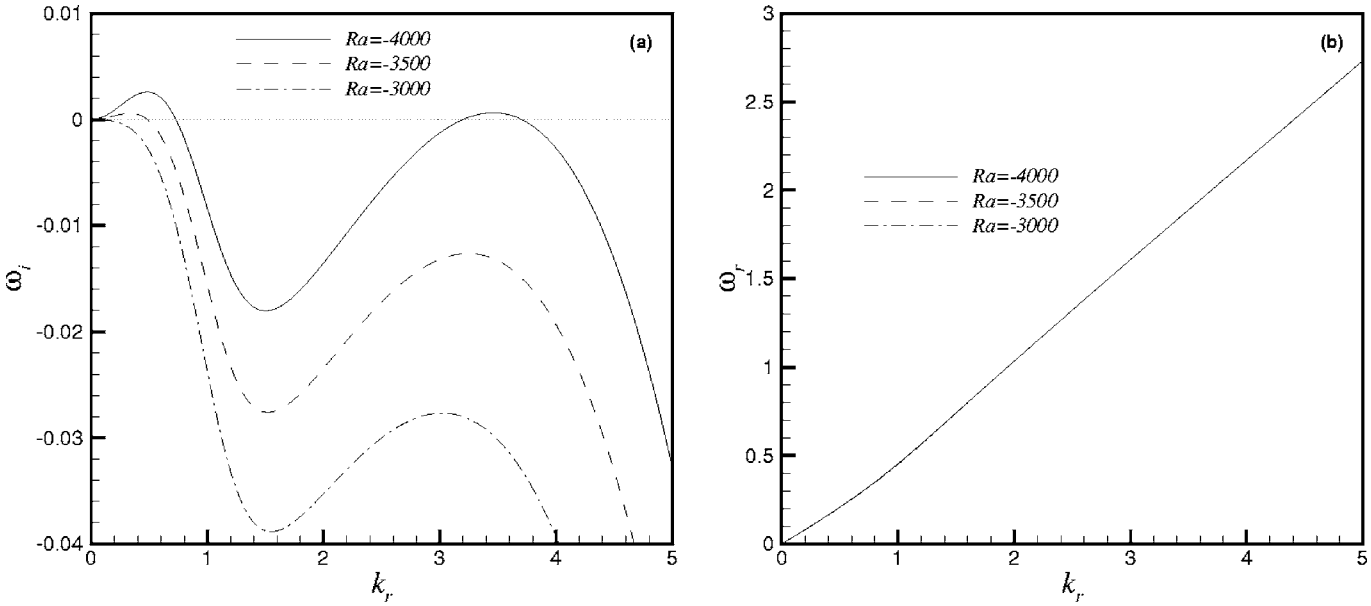

FIG. 8. Temporal growth rates and frequencies as functions of the wavenumber for different negative Rayleigh numbers (Re=0.04, ψ=−0.02, Pr=10, Le =0.01).

oscillatory instability. The wavenumbers and angular frequencies corresponding to this oscillatory instability are given in Figs. 9(c) and 9(d). They both do not depend much on ψ, except for the smallest values of $|\psi|$, and increase with the increase of Re. For the values of Re considered (Re =0.02 and Re=0.04), the wavenumbers have values quite similar to those obtained for Ra>0 and clearly different from zero (which is the value obtained at Re=0 and for the steady thresholds) whereas the angular frequencies are rather small.

IV. KINETIC-ENERGY BUDGET ANALYSIS

A deeper physical understanding of the instability mechanisms for the Poiseuille-Rayleigh-Bénard convection in binary mixtures with Soret effect can be gained by energy analyses. For that, a kinetic-energy balance is derived from the linear stability equations (7) and the corresponding boundary conditions (9): Equation (7b) is multiplied by $\hat{u}^*$, the complex conjugate of $\hat{u}$, and added to Eq. (7c), which is multiplied by $\hat{w}^*$, and after integration along z, the real part of the resulting equation is taken. After some transformations to eliminate zero terms such as the pressure integral, the following relationship for the rate of change of the fluctuating kinetic energy E_k is then obtained:

$$\frac{dE_k}{dt} = E_i + E_d + E_{bt} + E_{bc}, \tag{10}$$

with

$$E_k = \frac{1}{2}\int_0^1 (|\hat{u}|^2 + |\hat{w}|^2)\, dz,$$

$$E_i = -\frac{1}{2}\int_0^1 (\hat{u}^*\hat{w} + \hat{u}\hat{w}^*)\, dz,$$

$$E_d = -\,\mathrm{Pr}\int_0^1 [|D\hat{u}|^2 + |D\hat{w}|^2 + k^2(|\hat{u}|^2 + |\hat{w}|^2)]\, dz,$$

$$E_{bt} = \frac{\mathrm{Pr}\cdot\mathrm{Ra}}{2}\int_0^1 (\hat{w}^*\hat{\theta} + \hat{w}\hat{\theta}^*)\, dz,$$

$$E_{bc} = \frac{\mathrm{Pr}\cdot\mathrm{Ra}}{2}\int_0^1 \psi(\hat{w}^*\hat{c} + \hat{w}\hat{c}^*)\, dz,$$

where E_i is the production of fluctuating kinetic energy by shear of mean flow, E_d is the viscous dissipation, and E_{bt} and E_{bc} are the thermal and solutal buoyancy contributions, respectively. It is clear that E_d is negative indicating that the viscous dissipation produces a stabilization effect. At the onset of the instability, the rate of change of the fluctuating kinetic energy E_k is zero, so that, by dividing by $|E_d|$, we can obtain

$$\frac{E_i}{|E_d|} + \frac{E_{bt}}{|E_d|} + \frac{E_{bc}}{|E_d|} = 1. \tag{11}$$

A. Ra>0 and ψ>0

For positive separation factors $\psi>0$, we first plot the different contributions to the kinetic-energy budget for ψ =0.1 and ψ=0.2 in Fig. 10 (the values of ψ chosen here belong to the solutal-dominated regime). We see that E_{bt} and E_{bc} (the thermal and solutal buoyancy contribution) have key destabilizing effects while E_i (the inertial contribution) has only a little stabilizing effect. When the Reynolds number is small, the solutal buoyancy contribution E_{bc} is much larger than the thermal buoyancy contribution E_{bt}. When Re is

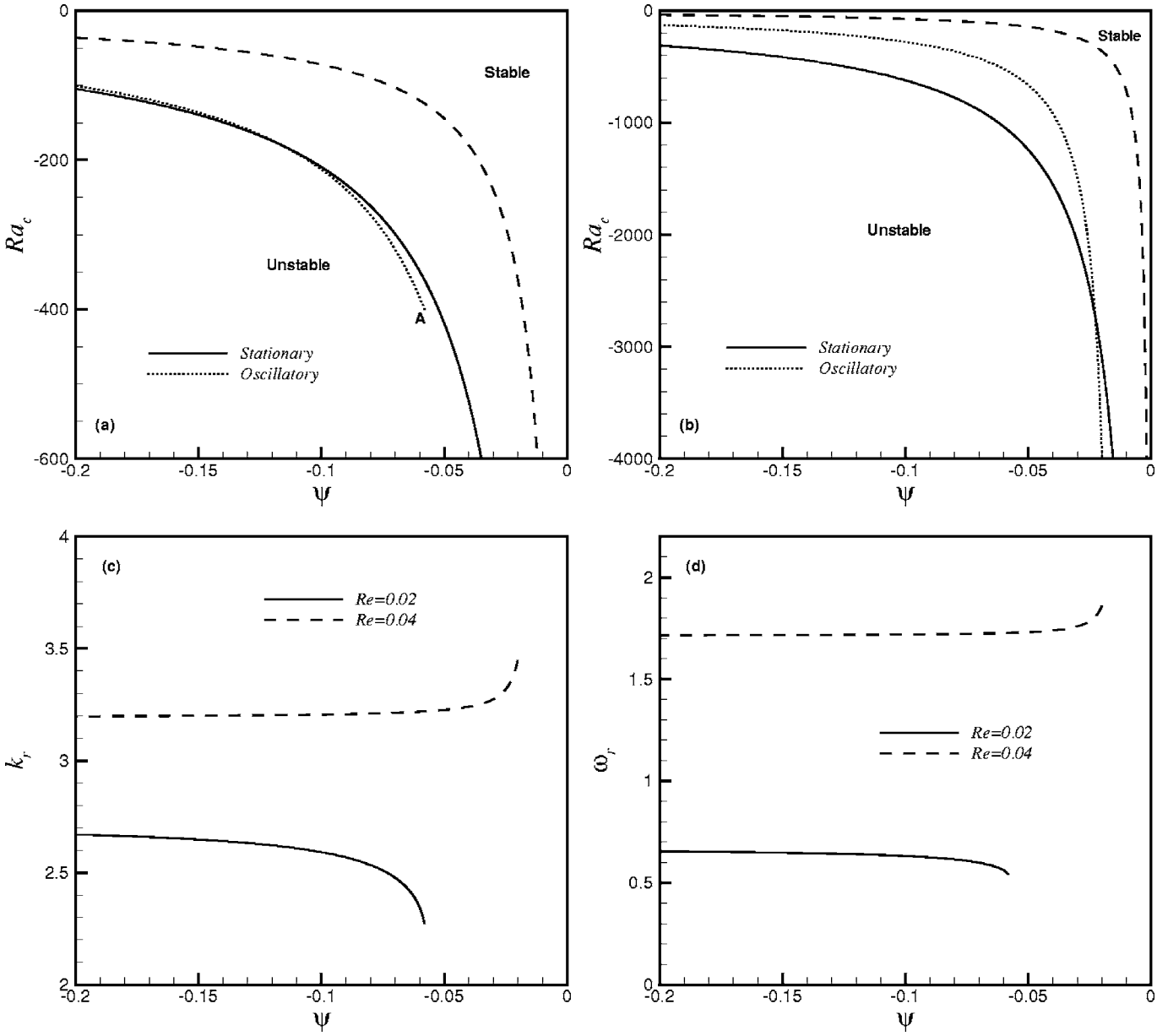

FIG. 9. Stationary and oscillatory critical curves for negative Rayleigh numbers [(a) Re=0.02, (b) Re_e=0.04], (c) real wavenumber k_r, and (d) angular frequency ω_r, for the oscillatory instability, as a function of the separation factor ψ (Pr=10, Le=0.01). The dashed curve in (a) and (b) represents the stationary thresholds at Re=0.

increased, the thermal buoyancy contribution increases and eventually becomes larger than the solutal buoyancy contribution which decreases. So, for small Reynolds numbers, the destabilization mainly comes from the solutal buoyancy part, while for large enough Reynolds numbers the destabilization mainly comes from the thermal buoyancy part. Note that there is a jump in the buoyancy contributions at the value of Re corresponding to the discontinuous change of slope for the Ra critical curves [Fig. 3(a)], and that the solutal buoyancy contributions evolve at large Re to asymptotic values clearly different from zero.

For the different kinetic-energy contributions, we give their distribution along the vertical direction for different Reynolds number at ψ=0.1 in Fig. 11. We can see that the inertial contribution is small everywhere, the viscous dissipation has peak values close to the top and bottom walls, and the thermal and solutal buoyancy contributions are mainly distributed in the middle of the channel where the flow is weaker. For Re=1.0, the destabilizing effect of the solutal buoyancy is larger than that of the thermal buoyancy. For Re=1.5, the two destabilizing effects have nearly same intensities. Finally for Re=2.0, the thermal buoyancy has the main destabilizing effect. This change is connected to a clear decrease of the destabilizing solutal buoyancy energy when the Reynolds number is increased. Even so, this solutal contribution remains effective and appears as two symmetrically arranged peaks on both sides of the horizontal midplane of the cavity. These peaks are connected to two maxima in the fluctuating concentration field. These maxima appear from

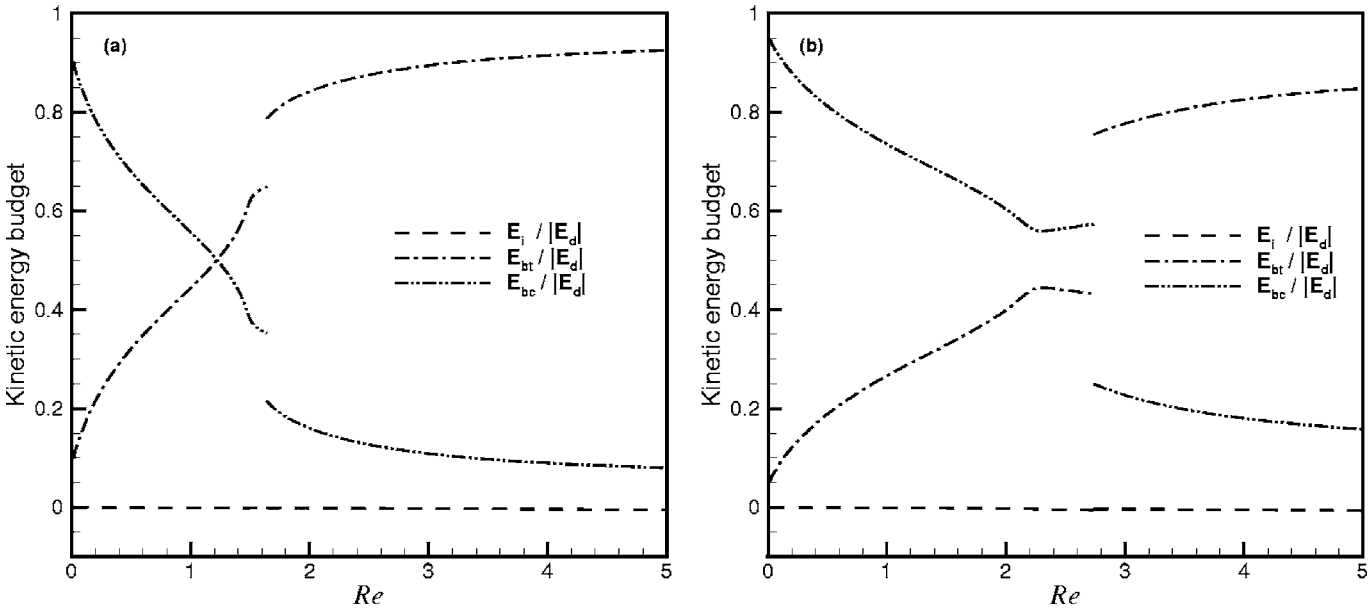

FIG. 10. Different contributions (from inertia, thermal, and solutal buoyancy) to the kinetic-energy budget at the critical thresholds as a function of the Reynolds number for (a) $\psi=0.1$ and (b) $\psi=0.2$ (Ra$>$0, Pr=10, Le=0.01).

the arrowhead-like maximum contour line given in Fig. 13 (Re=0.6) of Jung *et al.*[2] when Re is further increased.

B. Ra>0 and $\psi<0$

For negative separation factors $\psi<0$, we plot the different contributions to the kinetic-energy budget for $\psi=-0.1$ and $\psi=-0.2$ in Fig. 12. The solutal buoyancy contribution is found to be negative indicating a stabilizing contribution, the inertial contribution is very small, really negligible, and the thermal buoyancy contribution is the main destabilizing effect. With the increase of the Reynolds number, the stabilization from the solutal buoyancy contribution becomes stronger, which implies a more destabilizing contribution from the thermal buoyancy at onset. From the figure, it is also seen that the initial change with Re of the different contributions is slower for the downstream mode than for the upstream mode. Then, when the Reynolds number is larger, the change of the contributions for the downstream mode continues to increase, while the contributions for the upstream mode levels off quickly and then evolve towards an asymptotic value.

The distributions of the different kinetic-energy contributions along the vertical direction are shown in Fig. 13 for $\psi=-0.1$ and two values of Re. The distributions for the inertial, viscous dissipation, and thermal buoyancy contributions are similar to those obtained for positive ψ. For Re =0.5, the true critical Rayleigh number is determined by the downstream mode for which, as seen in Fig. 13(a), the rather small stabilizing solutal buoyancy contribution is effective in the middle of the channel. But for Re=1.0, the true critical Rayleigh number is determined by the upstream mode for which, as seen in Fig. 13(b), this contribution is distributed symmetrically on both sides of the horizontal midplane, the two peaks being a little more apart than for $\psi>0$ in Fig.

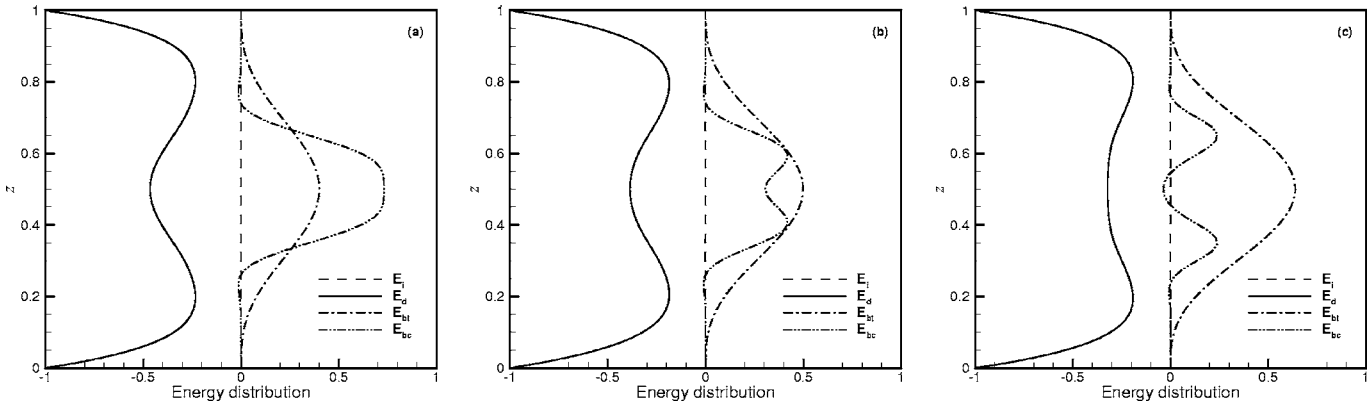

FIG. 11. Energy distribution along the vertical direction z for the different contributions (from inertia, viscous dissipation, thermal, and solutal buoyancy) at the critical thresholds for (a) Re=1.0, (b) Re=1.5, and (c) Re=2.0 (Ra$>$0, $\psi=0.1$, Pr=10, Le=0.01).

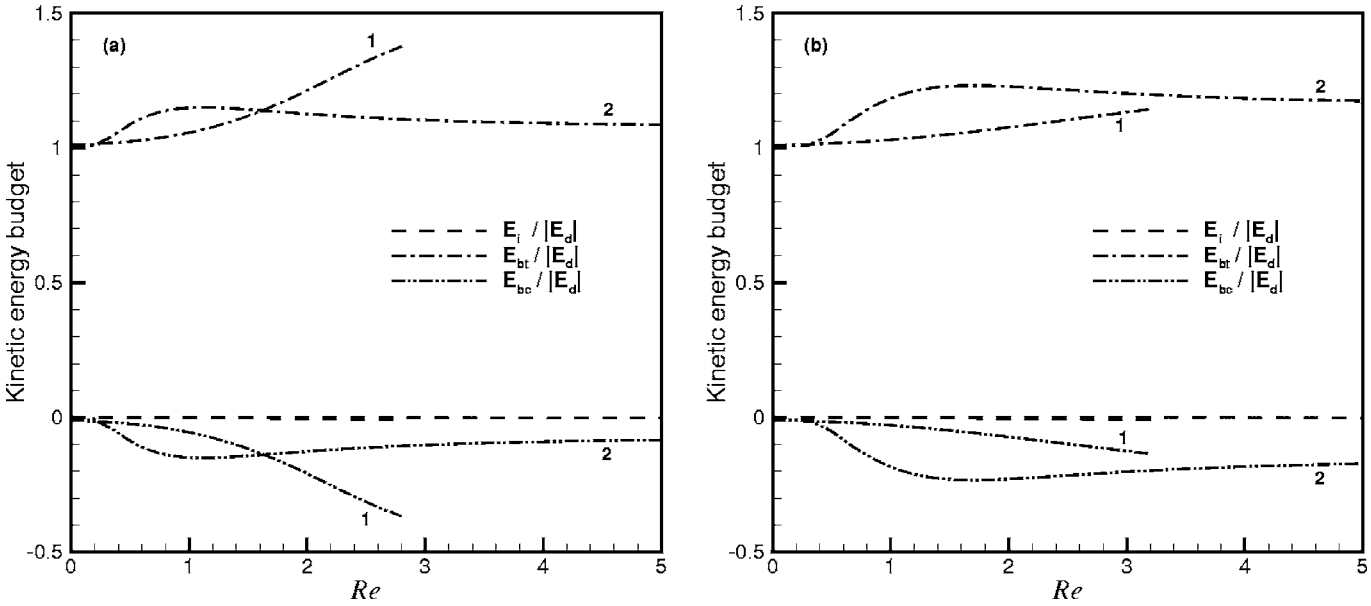

FIG. 12. Different contributions (from inertia, thermal, and solutal buoyancy) to the kinetic-energy budget at the critical thresholds as a function of the Reynolds number for (a) $\psi=-0.1$ and (b) $\psi=-0.2$ (Ra$>$0, Pr=10, Le=0.01). Line 1 corresponds to downstream modes and line 2 to upstream modes.

11(c). These peaks are connected to two maxima in the fluctuating concentration field which were already visible in Fig. 11 (Re=0.6) of Jung *et al.*[2]

C. Ra<0

For Ra$<$0, the different contributions to the kinetic-energy budget are given for the oscillatory transition at $\psi=-0.1$ and $\psi=-0.2$ in Fig. 14. In this case the main destabilizing contribution comes from the solutal buoyancy contribution, whereas the thermal buoyancy contribution is stabilizing. These contributions increase almost linearly with the increase of Re, in connection with the increase of the thresholds Ra_c. For larger $|\psi|$, the increase of these contributions with Re is smaller, as was the increase of the thresholds. Looking to the distribution of the different kinetic-energy contributions given in Fig. 15 for $\psi=-0.1$, we see that the thermal and solutal buoyancy contributions are clearly distributed in the middle of the channel, with a dominant contribution from the destabilizing solutal effect. When Re is increased (or $|\psi|$ decreased), both peaks increase in size, the increase of the destabilizing solutal buoyancy contribution compensating for the increase of the stabilizing thermal buoyancy contribution. Note that when the thresholds are stationary (Re=0, or Re small and $|\psi|$ large), the

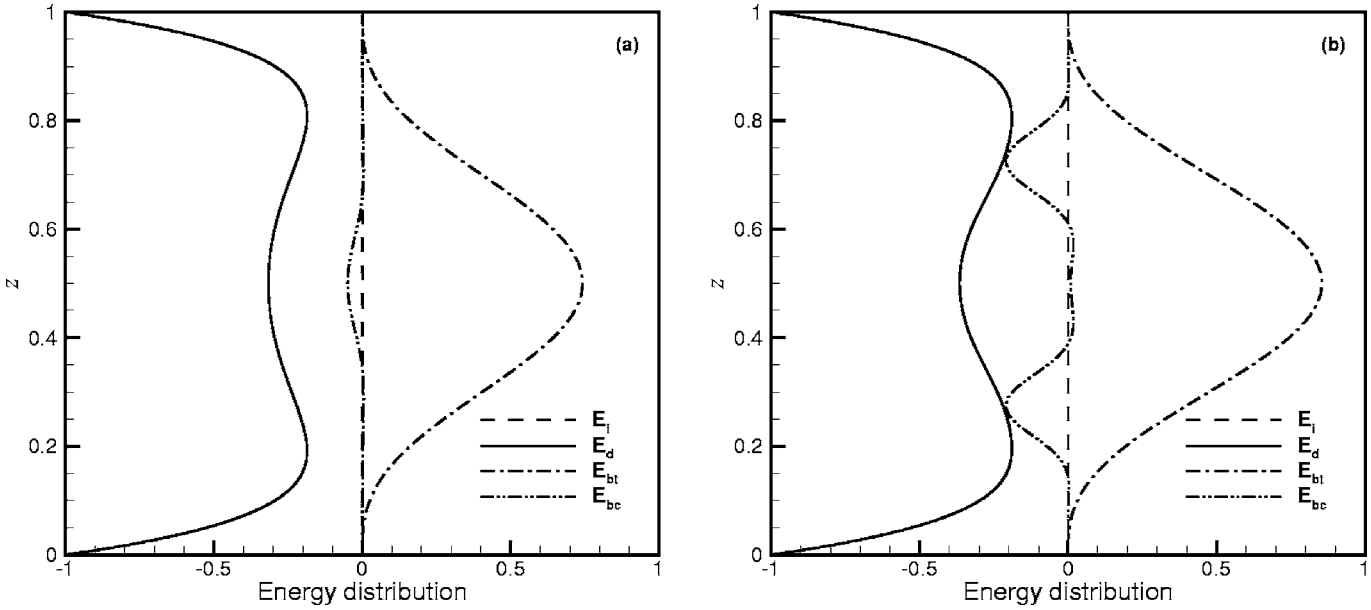

FIG. 13. Energy distribution along the vertical direction z for the different contributions (from inertia, viscous dissipation, thermal, and solutal buoyancy) at the critical thresholds for (a) Re=0.5 (downstream mode) and (b) Re=1.0 (upstream mode) (Ra$>$0, $\psi=-0.1$, Pr=10, Le=0.01).

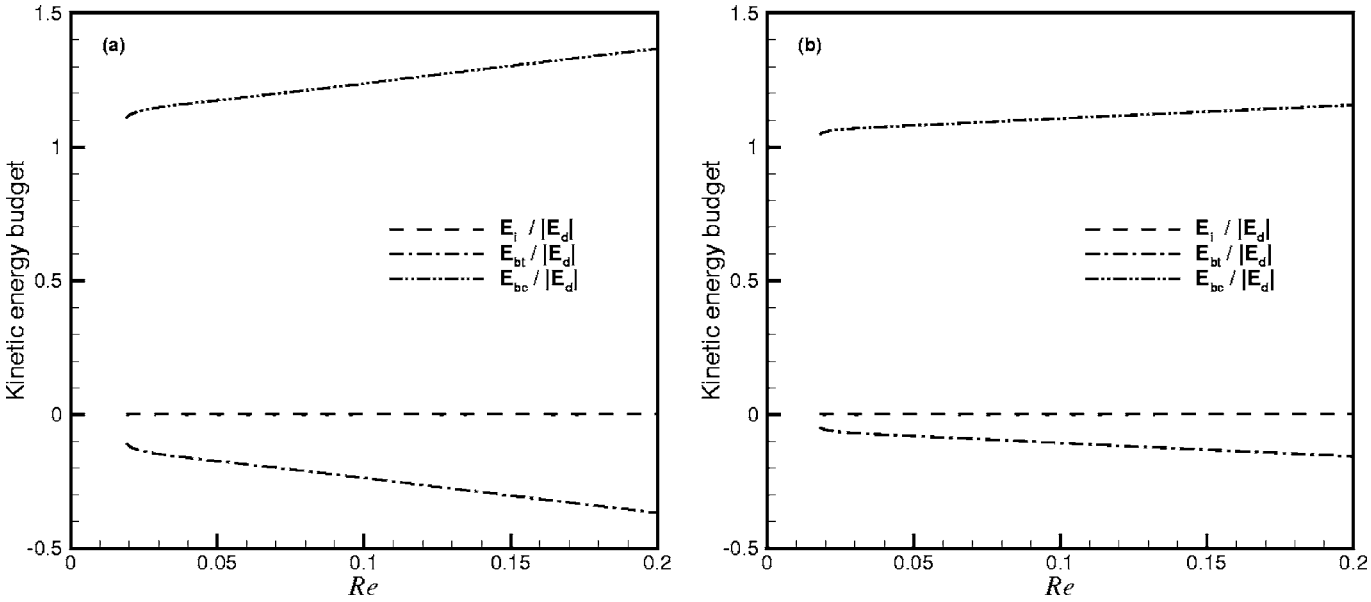

FIG. 14. Different contributions (from inertia, thermal, and solutal buoyancy) to the kinetic-energy budget at the critical thresholds as a function of the Reynolds number for (a) $\psi=-0.1$ and (b) $\psi=-0.2$ ($\mathrm{Ra}<0$, $\mathrm{Pr}=10$, $\mathrm{Le}=0.01$).

instability, which occurs at $k_r^c=0$, is triggered by a pure destabilizing solutal buoyancy contribution, without any thermal buoyancy contribution.

V. ABSOLUTE AND CONVECTIVE INSTABILITY

Before we consider the spatiotemporal instability of the Poiseuille-Rayleigh-Bénard flows, let us recall the basic concepts of the absolute/convective instability theory (AI/CI) which originated from plasma physics.[15,16] A good introduction to this theory can be found in Huerre and Monkewitz,[17,18] who first applied such a spatiotemporal stability analysis to spatially developing flows. They analytically investigated the absolute/convective nature of the instability through the asymptotic response of Green's function at large time. Furthermore, they indicated that periodic forcing on the boundary can be spatially amplified only when the system is convectively unstable.

Basically, when an amplifying wave packet is convected away from its local position, the wave packet would be said to be convectively unstable. If, otherwise, the amplification can be observed locally, the wave packet would be said to be absolutely unstable. Generally, the absolute/convective nature of the instability is determined by the sign of the absolute growth rate $\omega_{0i}=\mathrm{Im}[\omega(k_0)]$ defined at the saddle point k_0

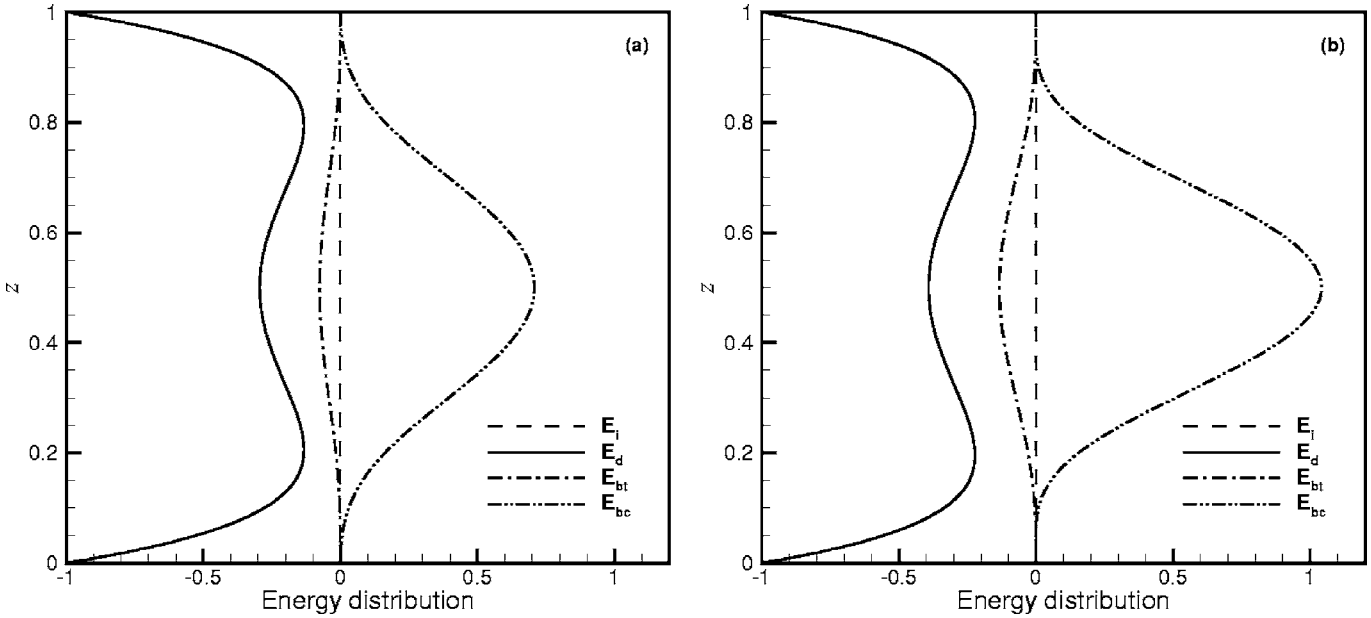

FIG. 15. Energy distribution along the vertical direction z for the different contributions (from inertia, viscous dissipation, thermal, and solutal buoyancy) at the critical thresholds for (a) $\mathrm{Re}=0.02$ and (b) $\mathrm{Re}=0.04$ ($\mathrm{Ra}<0$, $\psi=-0.1$, $\mathrm{Pr}=10$, $\mathrm{Le}=0.01$).

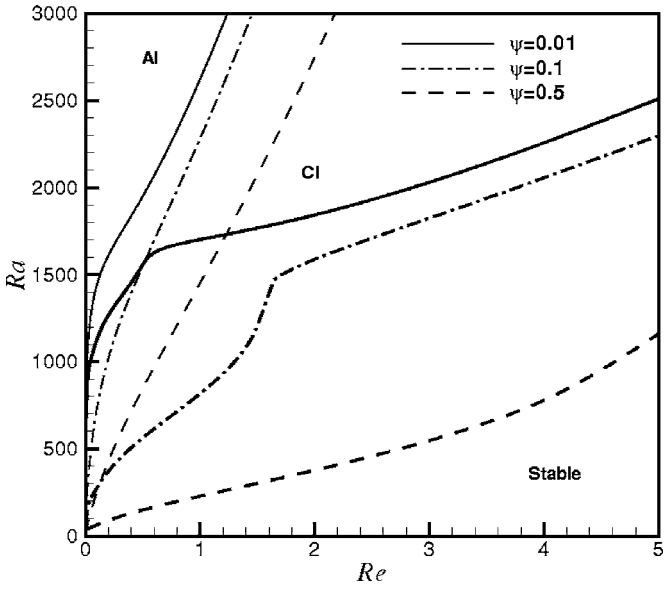

FIG. 16. AI/CI boundary curves (thin lines) and critical Rayleigh number curves (thick lines) as a function of the Reynolds number for different positive values of the separation factor ψ (Pr=10, Le=0.01).

of the dispersion relation, i.e., when $\frac{d\omega}{dk}|_{k_0}=0$. In these expressions, k is a complex wavenumber and ω is a complex frequency. If the absolute growth rate ω_{0i} is greater than zero (lower than zero), the flow is said to be absolutely (convectively) unstable, and the boundary between absolute and convective instability is then determined by a zero absolute growth rate, i.e., $\omega_{0i}=0$. But it should be noticed that the saddle point k_0 used to identify AI/CI must satisfy the Briggs-Bers collision criterion, i.e., the saddle point must be a pinch point produced by two distinct spatial branches of solutions of the dispersion relation, $k_n^{\pm}(\omega)$, coming, respectively, from the upper and lower half k planes, and commonly referred to as upstream and downstream branches. In this paper the saddle points have all been found to satisfy the collision criterion.

A. Ra>0

In Figs. 16 and 17, we plot the boundary curves between absolute and convective instability together with the critical curves for the onset of convection as functions of the Reynolds number for different values of the separation factor ψ, in the case where heating is from below (Ra>0). We see that the parameter region is partitioned into three parts, i.e., the stable, convectively unstable, and absolutely unstable regions. For positive separation factors (Fig. 16), the critical Rayleigh number where the stable region directly changes into the absolutely unstable region occurs at zero Reynolds number. Differently, for a negative separation factor [$\psi=-0.1$ in Fig. 17], such a critical Rayleigh number occurs at a nonzero moderate Reynolds number. In the paper of Jung *et al.*,[2] it is pointed out that the AI/CI boundary curve first decreases with the increase of the Reynolds number, coincides at its local minimum with the critical curve, and afterwards increases with the Reynolds number. We agree with their conclusions except that, as can be seen in Fig. 17(b), the contact point between the AI/CI boundary curve and the critical curve seems not to be the local minimum of the AI/CI boundary curve.

In order to clearly define the characteristics of the unstable flow near that critical Rayleigh number, it is necessary to study the response of the flow to a localized disturbance along an arbitrary fixed spatiotemporal ray, $V=x/t$, as $t\to\infty$. This is equivalent to analyzing how the response evolves in a reference frame moving at the velocity V. Upon introducing

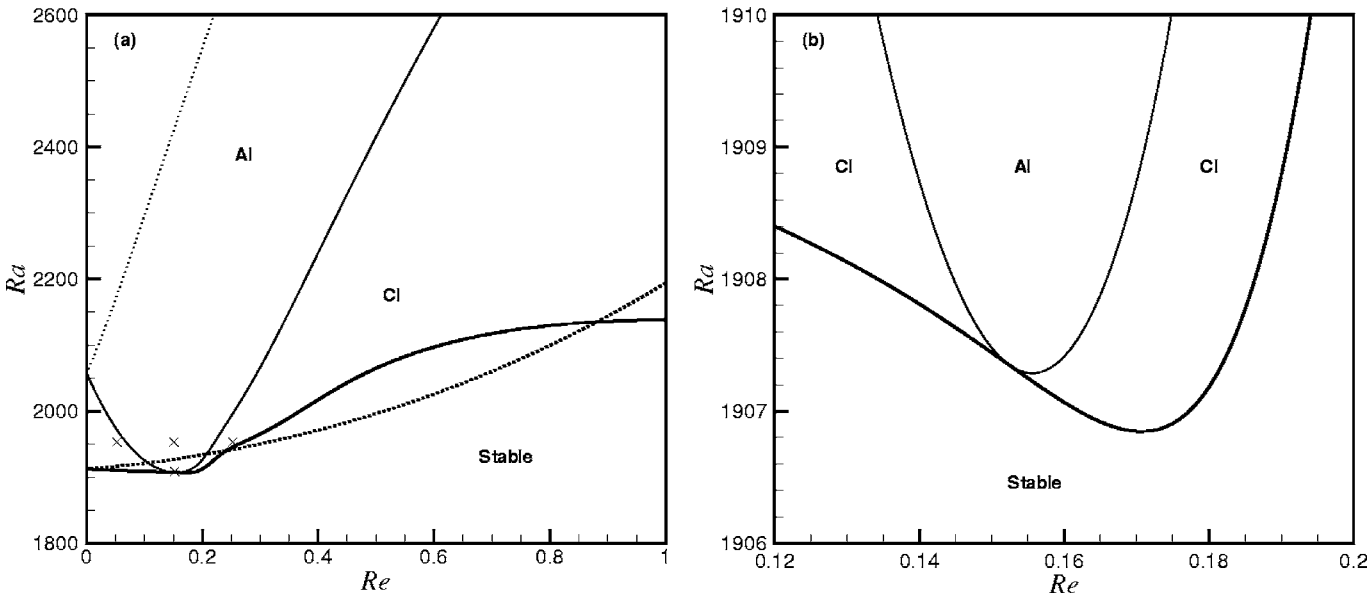

FIG. 17. AI/CI boundary curves (thin lines) and critical Rayleigh number curves (thick lines) as a function of the Reynolds number for $\psi=-0.1$ (Pr=10, Le=0.01). (a) Global view showing the curves for both upstream (solid lines) and downstream (dotted lines) modes. (b) Detailed view close to the contact point between the AI/CI boundary curve and the critical curve for the upstream mode. Crosses (×) in (a) indicate points in the (Ra,Re) parameter space at which growth rates will be plotted in Fig. 18.

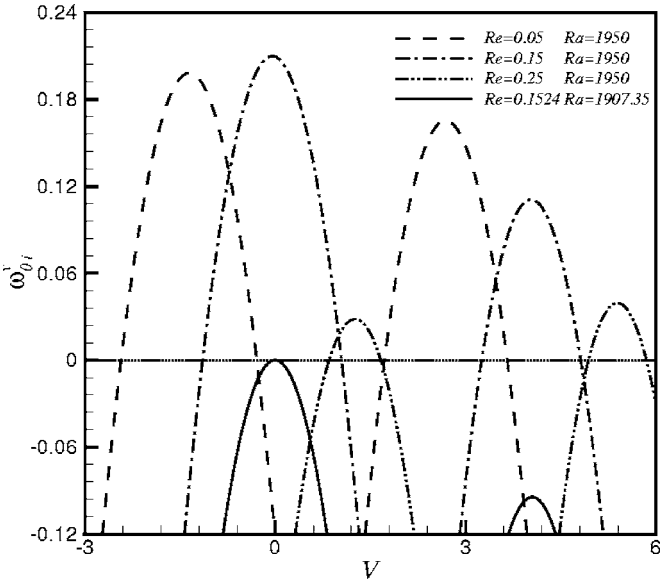

FIG. 18. Growth rate ω^v_{0i} as a function of the ray velocity V at different points in the (Ra,Re) parameter space indicated by a cross (×) in Fig. 17 for $\psi=-0.1$ (Pr=10, Le=0.01).

the Doppler-shifted frequency $\omega^v=\omega-Vk$ and $k^v=k$, the dispersion relation in the moving coordinate system would be

$$D_v(k^v,\omega^v)=D(k^v,\omega^v+Vk^v)=0. \tag{12}$$

Due to $d\omega^v/dk^v=0$, the saddle point $\tilde{k}$ will take place at

$$D(\tilde{k},\tilde{\omega})=0 \quad \text{and} \quad \frac{d\omega}{dk}(\tilde{k},\tilde{\omega})=V, \tag{13}$$

and then the absolute growth rate in the moving frame is obtained at $k_0^v=\tilde{k}$ through

$$\omega_0^v=\tilde{\omega}-V\tilde{k}. \tag{14}$$

Here also, the saddle point $\tilde{k}$ obtained from (13) must verify the Briggs-Bers collision criterion mentioned above.

For the values of Rayleigh and Reynolds numbers defined by a cross (×) in Fig. 17(a), we plot the growth rate ω^v_{0i} as a function of the ray velocity V for $\psi=-0.1$ in Fig. 18. When Re=0.05 and Ra=1950, the left and right traveling waves are convected upstream and downstream, respectively, for their unstable growth rates have peaks, respectively, on the left and right sides of $V=0$. When Re=0.15 and Ra=1950, the right traveling wave is still convected downstream with faster velocity and smaller growth rate, but the left traveling wave, with a little larger growth rate, is now absolutely unstable because the growth rate at $V=0$ is larger than zero, i.e., the absolute growth rate is greater than zero. Furthermore, when Re=0.25 and Ra=1950, the left traveling wave is convected downstream with a smaller growth rate as well as the right traveling wave. This transition process observed at fixed Rayleigh number shows that large enough mean flow forces the localized perturbations to convect all downstream. For Re=0.1524 and Ra=1907.35, we see that the maximal growth rate of the left traveling wave is zero and just located at the origin of the reference frame. This means that this maximal growth rate is also an absolute growth rate. So the point corresponding to Re=0.1524 and Ra=1907.35 is the contact point which is located on both the critical Rayleigh number curve and the AI/CI boundary curve, as shown in Fig. 17. Then across this point, i.e., for Ra>1907.35 when Re=0.1524, the stable system is directly changed into an absolutely unstable state through the left traveling wave.

It is interesting to determine such transition points for different separation factors. For that, we first plot the absolute growth rate ω_{0i}, the absolute oscillatory frequency ω_{0r}, the absolute spatial amplification rate $-k_{0i}$, and the absolute spatial wavenumber k_{0r} as functions of Re when moving along the critical Rayleigh number curve and along the AI/CI boundary curve (both determined by the left traveling wave) for the separation factor $\psi=-0.1$ (Fig. 19). As shown in Fig. 19(a), the absolute growth rates ω_{0i} along the critical curve are all less than or equal to zero. The corresponding curve first increases with increasing Reynolds number, reaches a local maximum in contact with the real axis (which is the curve for the AI/CI boundary), and then decreases when Re is further increased. Concerning the absolute angular frequencies ω_{0r} along both the critical curve and the AI/CI boundary curve [Fig. 19(b)], they increase with Reynolds number and cross the real axis, but the contact point is a little below the real axis. The absolute amplification rates $-k_{0i}$ also increase with Reynolds number [Fig. 19(c)], but now the contact point is exactly on the real axis. Note that the two curves shown in Figs. 19(b) and 19(c) are very close (nearly identical) near the contact point. Finally, as shown in Fig. 19(d), the absolute spatial wavenumber k_{0r} of the AI/CI boundary curve is always above that of the critical curve except for very small Reynolds numbers.

From the properties deduced from Fig. 19, we see that the contact point can be determined by either the local maximum of the absolute growth rate along the critical curve or the zero value of the absolute spatial amplification rate along the critical curve or along the AI/CI boundary curve. Among these three possible algorithms to compute the contact point, we have adopted the computation of the zero value of the absolute amplification rate along the critical curve. The loci of the contact points for different negative separation factors (from 0 to −0.5) are plotted in Fig. 20. We see that with the increase of the absolute value of the separation factor, the critical Rayleigh number and the corresponding Reynolds number at the contact point both increase. Numerical data for these contact points are also given in Table I.

B. Ra<0

In the case where heating is from above (Ra<0), the boundary between absolute and convective instability can also be determined. The corresponding curves connected for $\mathrm{Re}\neq 0$ to the oscillatory instability shown in Fig. 9 are given in Fig. 21, first as a function of ψ for different Re values [Fig. 21(a)] and then as a function of Re for different ψ values [Fig. 21(b)]. As it was found for the critical curves in Fig. 9, the boundary curves evolve from the curve at Re=0 (which corresponds to the steady transition occurring with $k_r^c=0$) towards larger |Ra| and $|\psi|$ when the Reynolds number

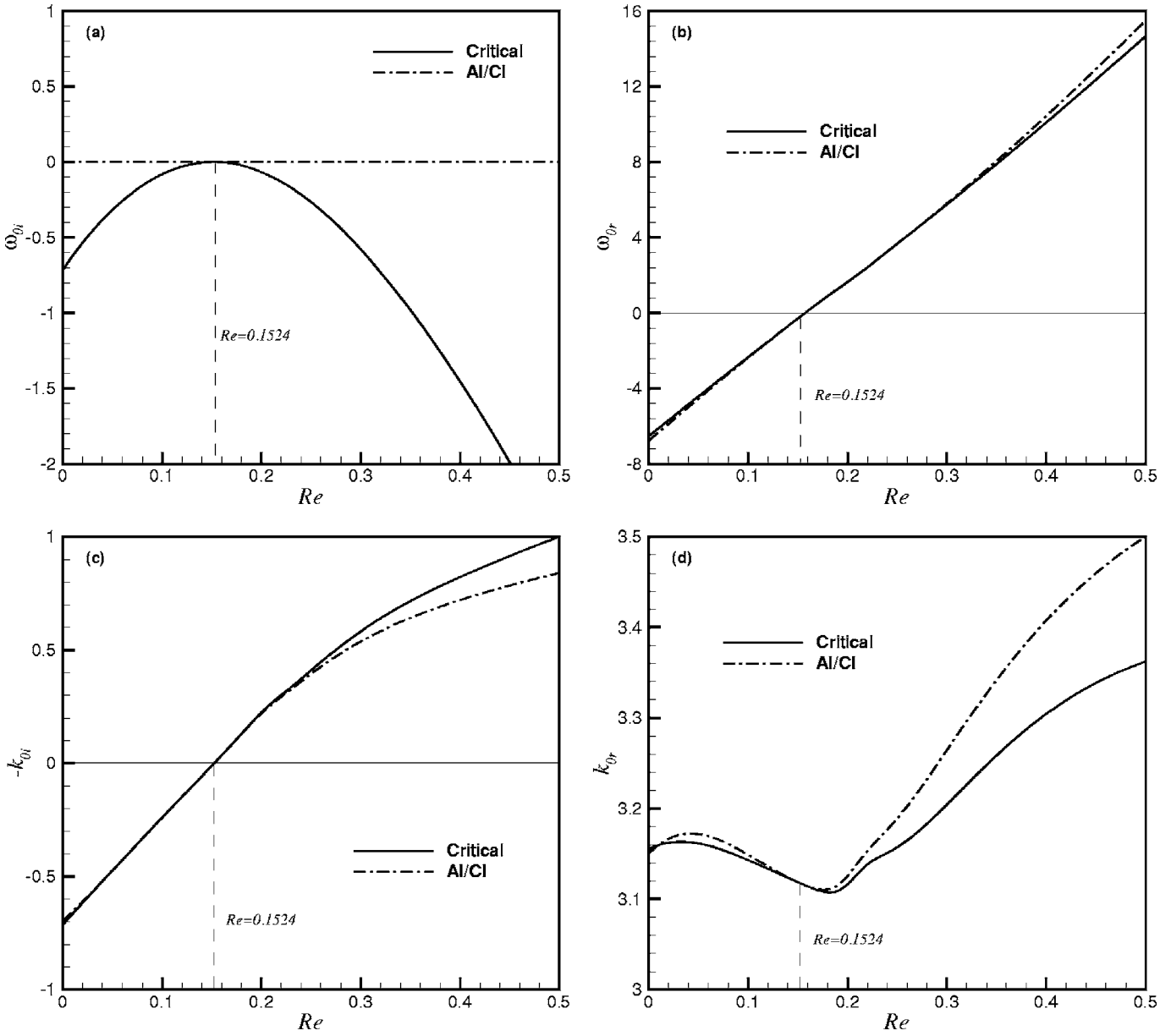

FIG. 19. (a) Absolute growth rate ω_{0i}, (b) absolute oscillatory frequency ω_{0r}, (c) absolute spatial amplification rate $-k_{0i}$, and (d) absolute spatial wavenumber k_{0r} as a function of the Reynolds number along the critical Rayleigh number curve and along the AI/CI boundary curve for the upstream mode ($\psi=-0.1$, Pr=10, Le=0.01).

is increased [Fig. 21(a)]. This means that for large Re and small $|\psi|$, it will be difficult to make the system absolutely unstable, i.e., a high-temperature difference between the upper and the lower walls will be needed. The great sensitivity of the boundary curves to the Reynolds number is more clearly shown in Fig. 21(b). This sensitivity is still more effective for small values of $|\psi|$.

VI. CONCLUSION

In this paper, the linear stability of Poiseuille-Rayleigh-Bénard flows in binary fluids with Soret effect is analyzed for a large Reynolds number range by a pseudospectral collocation method. It is well known that in the situation where heating is from below ($\mathrm{Ra}>0$), for positive separation factors and without throughflow there is a cutoff separation factor ψ_c above which the critical Rayleigh number for the onset of the stationary instability occurs at zero wavenumber. When a throughflow is applied, this cutoff separation factor is strongly affected, becoming quickly large with the increase of the Reynolds number. As a consequence, for the separation factors $\psi>\psi_c$, a small Reynolds number can change the critical wavenumber from zero to a finite value. Furthermore, for large enough positive separation factors, there exists a Reynolds number range where three local minima occur in the neutral curves $\mathrm{Ra}(k)$. This induces a discontinuous change of slope in the evolution of the critical Rayleigh number with Re together with a jump of the critical wavenumber and of the critical angular frequency. For $\mathrm{Ra}>0$ and negative separation factors, the type of convection which bifurcates out of the conductive state changes when Re is in-

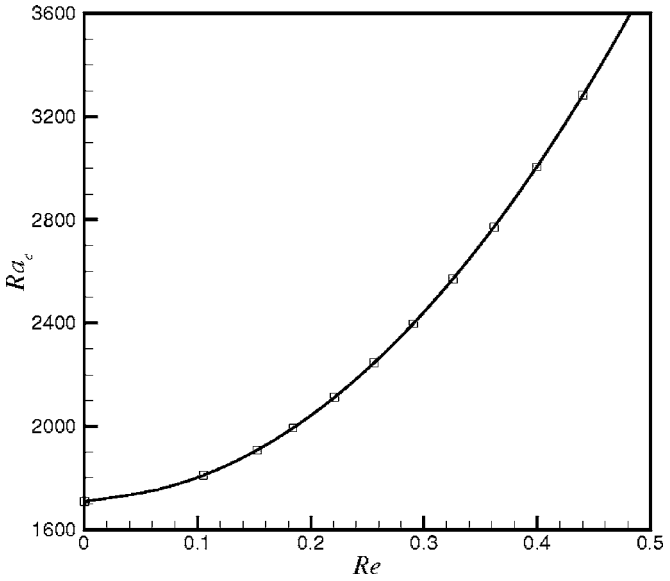

FIG. 20. Contact points between AI/CI boundary curves and critical curves (upstream mode) expressed in the (Ra_c,Re) parameter space for different separation factors ψ. The square symbols from left to right correspond to $\psi=-0.05\times n$ for $n=0$ to 10 (Pr=10, Le=0.01).

creased. At small Re, convection appears on the so-called upstream branch, first as an upstream traveling wave which then evolves towards a downstream traveling wave. At intermediate Re, convection changes to a faster downstream traveling wave belonging to the downstream branch. Finally, at larger Re, convection changes again to a slower downstream traveling wave belonging to the upstream branch. In this case too, the thresholds remain influenced by the solutal effect even at large Re (Re=5). In the situation where heating is from above ($Ra<0$), the stationary critical curve obtained at Re=0 is replaced by two critical curves, one stationary and the other oscillatory, when a throughflow is applied. The

TABLE I. Critical Rayleigh number and corresponding Reynolds number at the contact point between the critical curve and the AI/CI boundary curve for different negative separation factors ψ (Pr=10, Le=0.01).

ψ	Re	Ra_c
−0.01	0.045 956 7	1737.748 53
−0.05	0.105 025 9	1809.689 31
−0.1	0.152 434 7	1907.348 17
−0.2	0.227 997 6	2137.343 54
−0.3	0.297 404 1	2429.945 25
−0.4	0.369 078 3	2815.013 99
−0.5	0.448 873 9	3344.645 13

thresholds $|Ra_c|$ are found to increase for both instabilities when Re is increased, the oscillatory instability quickly becoming the dominant instability.

A kinetic-energy budget analysis for the binary fluid system is also performed. From it, it is clear that for $Ra>0$ when the separation factor is positive the solutal buoyancy contribution is destabilizing, reinforcing the destabilizing thermal buoyancy contribution whereas when the separation factor is negative this contribution is stabilizing. An increase of the Reynolds number induces a decrease of the solutal buoyancy contribution, in agreement with the diminution of the vertical convective transport of concentration perturbations due to the imposed throughflow,[2] but these solutal buoyancy contributions remain effective on both sides of the layer midplane. For $Ra<0$, the destabilization comes from the solutal buoyancy contribution whereas the thermal buoyancy contribution is stabilizing and an increase of Re induces an increase of both contributions.

Finally, the boundary curves between absolute and convective instability have been obtained for each of the situations studied. For $Ra>0$ and negative separation factors, it is shown that there is a contact point between the upstream

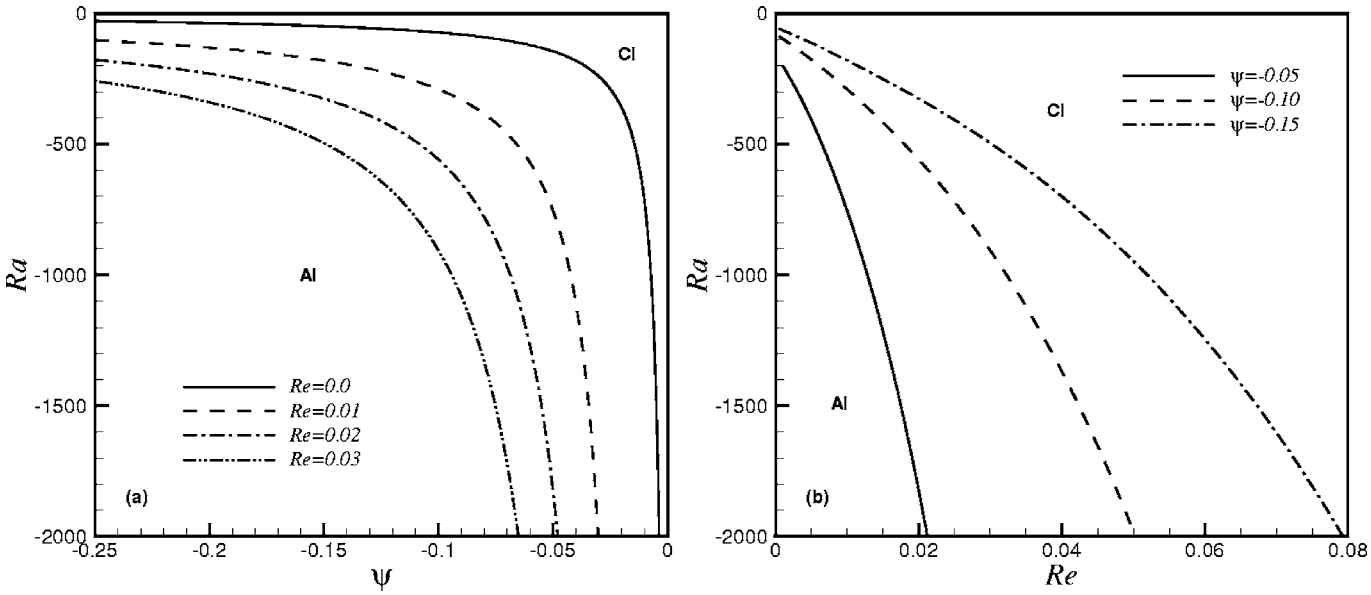

FIG. 21. AI/CI boundary curves as a function of ψ for different Reynolds numbers (a) and as a function of Re for different separation factors (b) ($Ra<0$, Pr=10, Le=0.01).

wave critical curve and the corresponding boundary curve. At this point, the system is directly changed from a stable region to an absolutely unstable region. These contact points have been clearly characterized and localized. They are given in the (Ra_c,Re) parameter space for different negative separation factors. For $Ra < 0$, the boundary curves are found to move to larger $|Ra|$ and $|\psi|$ when Re is increased.

ACKNOWLEDGMENT

This work was funded by a fellowship from the Région Rhône-Alpes (J.H.).

[1] M. C. Cross and P. C. Hohenberg, "Pattern formation outside of equilibrium," Rev. Mod. Phys. **65**, 851 (1993).
[2] Ch. Jung, M. Lücke, and P. Büchel, "Influence of through-flow on linear pattern formation properties in binary mixture convection," Phys. Rev. E **54**, 1510 (1996).
[3] P. Büchel and M. Lücke, "Influence of through flow on binary fluid convection," Phys. Rev. E **61**, 3793 (2000).
[4] P. Büchel and M. Lücke, "Localized perturbations in binary fluid convection with and without throughflow," Phys. Rev. E **63**, 016307 (2001).
[5] D. Jung and M. Lücke, "Traveling wave fronts and localized traveling wave convection in binary fluid mixtures," Phys. Rev. E **72**, 026307 (2005).
[6] C. Canuto, M. Y. Hussaini, A. Quarteroni, and T. A. Zang, *Spectral Methods in Fluid Dynamics* (Springer-Verlag, New York, 1988).
[7] E. Knobloch and D. R. Moore, "Linear stability of experimental Soret convection," Phys. Rev. A **37**, 860 (1988).
[8] M. C. Cross and K. Kim, "Linear instability and the codimension-2 region in binary fluid convection between rigid impermeable boundaries," Phys. Rev. A **37**, 3909 (1988).
[9] M. C. Cross and K. Kim, "Existence of a codimension-2 point at the threshold of binary-fluid convection between rigid, impermeable boundaries," Phys. Rev. A **38**, 529 (1988).
[10] W. Schöpf and W. Zimmermann, "Multicritical behaviour in binary fluid convection," Europhys. Lett. **8**, 41 (1989).
[11] W. Schöpf and W. Zimmermann, "Convection in binary fluids: Amplitude equations, codimension-2 bifurcation, and thermal fluctuations," Phys. Rev. E **47**, 1739 (1993).
[12] N. D. Stein, "Exact sine series solution for oscillatory convection in a binary fluid," Phys. Rev. A **43**, 768 (1991).
[13] W. Hort, S. J. Linz, and M. Lücke, "Onset of convection in binary gas mixtures: Role of the Dufour effect," Phys. Rev. A **45**, 3737 (1992).
[14] St. Hollinger and M. Lücke, "Influence of the Dufour effect on convection in binary gas mixtures," Phys. Rev. E **52**, 642 (1995).
[15] R. J. Briggs, *Electron-Stream Interaction with Plasmas* (MIT Press, Cambridge, MA, 1964).
[16] A. Bers, "Theory of absolute and convective instabilities," in *Survey Lectures, Proceedings of the International Congress on Waves and Instabilities in Plasmas*, edited by G. Auer and F. Cap (Institute for Theoretical Physics, Innsbruck, 1973), p. B1.
[17] P. Huerre and P. A. Monkewitz, "Absolute and convective instabilities in free shear layers," J. Fluid Mech. **159**, 151 (1985).
[18] P. Huerre and P. A. Monkewitz, "Local and global instabilities in spatially developing flows," Annu. Rev. Fluid Mech. **22**, 473 (1990).